Pergamon

Computers Math. Applic. Vol. 31, No. 10, pp. 55-65, 1996

0898-1221/96 \$15.00 + 0.00

S0898-1221(96)00052-1

Steady Viscous Flow in a Triangular Cavity by Efficient Numerical Techniques

M. LI AND T. TANG
Department of Mathematics and Statistics
Simon Fraser University
Burnaby, British Columbia, Canada V5A 1S6

(Received December 1995; accepted February 1996)

Abstract—Accurate and efficient calculations of the flow inside a triangular cavity are presented for high Reynolds numbers. The Navier-Stokes equations, expressed in a stream function and vorticity formulation, are solved numerically using finite differences on a transformed geometry. Second-order numerical boundary conditions are derived and Newton's iteration is employed to solve the nonlinear system resulting from the finite difference discretization. Aside from solving the equilateral triangular cavity problem, we have also been able to compute numerical solutions for scalene triangular cavity problems. Our coarse-mesh results for the equilateral triangular cavity problem are compared with finer mesh results in the literature and the agreement is good.

Keywords—Navier-Stokes equations, Triangular cavity, Reynolds numbers, Newton's iteration, Finite difference method.

1. INTRODUCTION

The problem of steady incompressible viscous flow within a driven cavity is of primary importance in computational fluid dynamics (see the Introduction in [1,2] and the references therein). The development of improved methods for solving the square cavity problem has also been a subject of concern to computational physicists for many years. Although there are still some minor discrepancies in the results, the square cavity problem has been essentially realized (see, e.g., [3-5]). As pointed out in [1], the results for the square cavity may not be applied to other important geometries such as a trapezoidal or a triangular cavity. Also, the latter shapes are more common in practice (see, e.g., [6-8]). There are also differences between the square cavity and the trapezoidal/triangular cavity in the application of the finite difference method. At the corners and boundaries of the latter shapes, problems arise if standard algorithms are applied directly. Numerical approximations for geometries more complicated than rectangular domains have been a subject of study for some time (see, e.g., [9-11]).

The problem under consideration is the steady motion of an incompressible viscous flow in a triangular cavity of arbitrary geometry. The main object of this study is the development of an accurate and efficient scheme for solving Navier-Stokes problems in triangular geometries. Recent calculations of the steady problem in an equilateral triangular cavity have been given in [1,2] for $R \leq 500$, where R is the Reynolds number. The fourth-order Navier-Stokes equations in terms of stream function were solved numerically using finite differences and a Newton-like iteration on a transformed geometry.

We are grateful to A. Karageorghis for many helpful comments and suggestions. This research was supported under the Natural Sciences and Engineering Research Council of Canada Grant OGP0105545.

Typeset by $\mathcal{A}_{\mathcal{M}}\mathcal{S}$-TEX

A second-order finite difference approximation for the fourth-order Navier-Stokes equations requires 13-point stencils at the interior points except those nearest the three corners where non-symmetric 18-point stencils have to be used. To impose these wide stencils near the boundary, fictitious points exterior to the boundaries have to be provided and special treatment on the hypotenuse and corner points of the triangle has to be employed. A successful strategy has been provided in [1,2] to solve the equilateral triangular cavity problem. In the present work, we propose an alternative approach based on the Navier-Stokes equations in terms of the stream function and vorticity. A geometric transformation handling triangles of arbitrary shape is also presented. One of the difficulties with the stream-function-vorticity formulation is that the correct boundary conditions for the vorticity are not clear, since both boundary conditions are in terms of the stream function. To enforce boundary conditions, we use the so-called computational boundary method in which the computation region under consideration is one-grid inside the physical domain (see, e.g., [12,13]). On the physical boundaries, stream function and its derivatives are provided by impermeable and nonslip conditions, but the vorticity values are neither taken into account nor required in numerical computations. This is in conformity with the arguments that no vorticity should be specified on the no-slip walls either physically or mathematically when using stream-function-vorticity formulations [14]. Numerical results suggest that solving the stream-function-vorticity equations seems more efficient than solving the fourth-order stream function equation. By using the former formulation, we are able to obtain accurate results for larger values of R with fairly coarse grid sizes.

The organization of the paper is as follows. In the next section, we transform the Navier-Stokes problem in an arbitrary triangle to an equivalent problem posed on a right isosceles triangle. In Section 3, we introduce numerical schemes with special attention to computational boundary conditions. Numerical results are presented in Section 4 and discussions are presented in the final section.

2. GEOMETRIC TRANSFORMATION AND MATHEMATICAL FORMULATIONS

A triangular driven cavity of general shape is given by locating its three vertices at $\overline{O}(A,0)$, $\overline{P}(0,H)$, and $\overline{Q}(rA,H)$, with the upper side moving to the right via a constant velocity U; see Figure 1a. By a simple linear transformation

$$\xi = \frac{x-A}{rA} + \frac{y}{rH}, \qquad \eta = \frac{A-x}{rA} + \frac{r-1}{rH}y, \tag{1}$$

it is transformed to a fundamental triangle with vertices $O(0,0)$, $P(0,1)$, $Q(1,0)$; see Figure 1b. Accordingly

$$x = (1-\eta+(r-1)\xi)\,A, \qquad y = (\eta+\xi)\,H. \tag{2}$$

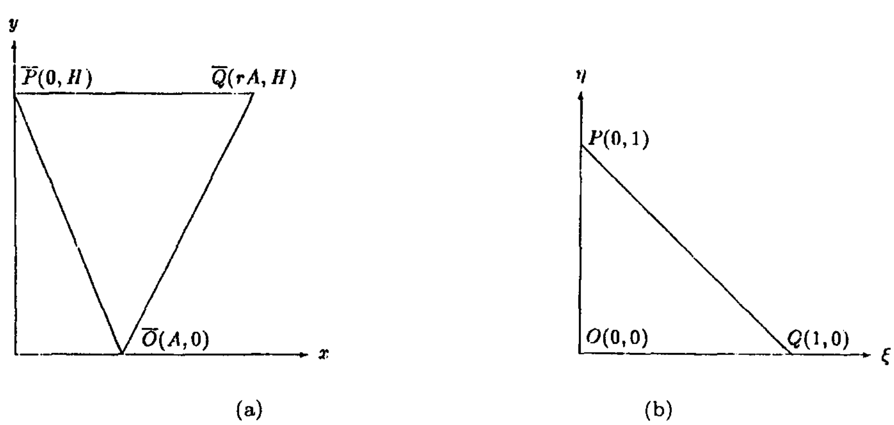

Figure 1. Geometric transformation.

The nondimensional Navier-Stokes equations and the continuity equation are reduced by introducing the stream function ψ and the vorticity ζ into

$$\begin{aligned} \psi_{xx} + \psi_{yy} &= -\zeta, \\ \zeta_{xx} + \zeta_{yy} &= \mathrm{R}\left(\psi_y \zeta_x - \psi_x \zeta_y\right). \end{aligned} \tag{3}$$

Here the variables are made dimensionless by one-third of the triangle height $H/3$ and the moving lid velocity U. The Reynolds number is defined as $\mathrm{R} = HU/3\nu$, where ν is the kinematic viscosity. The velocity components are defined by stream function as

$$u = \psi_y, \qquad v = -\psi_x.$$

Under transformation (1), the governing equations and velocity components in the $\xi\eta$-plane become

$$\left(1 + \frac{H^2}{A^2}\right)\psi_{\xi\xi} + 2\left(r - 1 - \frac{H^2}{A^2}\right)\psi_{\xi\eta} + \left((r-1)^2 + \frac{H^2}{A^2}\right)\psi_{\eta\eta} = -r^2 H^2 \zeta, \tag{4}$$

$$\left(1 + \frac{H^2}{A^2}\right)\zeta_{\xi\xi} + 2\left(r - 1 - \frac{H^2}{A^2}\right)\zeta_{\xi\eta} + \left((r-1)^2 + \frac{H^2}{A^2}\right)\zeta_{\eta\eta} = \frac{rH}{A}\mathrm{R}\left(\zeta_\xi \psi_\eta - \zeta_\eta \psi_\xi\right), \tag{5}$$

$$u = \frac{1}{rA}\left(\psi_\xi - \psi_\eta\right), \qquad v = \frac{1}{rH}\left(\psi_\xi + (r-1)\psi_\eta\right). \tag{6}$$

The boundary conditions in the xy-plane are

$$\psi = 0, \qquad \text{on all three sides,} \tag{7}$$

$$(u,v)\cdot\tau = \begin{cases} 1, & \text{for the top side,} \\ 0, & \text{for the other two sides,} \end{cases} \tag{8}$$

$$(u,v)\cdot n = 0, \qquad \text{on all three sides,} \tag{9}$$

where τ is the tangential unit vector pointing in the direction of motion (clockwise) and n is the outwards normal unit vector. In the $\xi\eta$-plane, condition (7) remains the same form while (8),(9) need to be converted as follows. On the top side $\overline{PQ}$, substituting (6) into (8),(9), with $\tau = (1,0)$, $n = (0,1)$ yields

$$\psi_\xi = \psi_\eta = H, \qquad \text{on side } \overline{PQ}. \tag{10}$$

On side $\overline{OP}$, we have

$$\tau = \frac{(-A, H)}{\sqrt{A^2 + H^2}}, \qquad n = \frac{(-H, -A)}{\sqrt{A^2 + H^2}}.$$

Combining this with (6), we convert (8),(9) into

$$\left(A^2 + H^2\right)\psi_\xi + \left(A^2(r-1) - H^2\right)\psi_\eta = 0, \qquad r\psi_\eta = 0.$$

Therefore,

$$\psi_\xi = \psi_\eta = 0, \qquad \text{on side } \overline{OP}. \tag{11}$$

Similarly, on side $\overline{QO}$ by using

$$\tau = \frac{((1-r)A, -H)}{\sqrt{(1-r)^2 A^2 + H^2}}, \qquad n = \frac{(H, (1-r)A)}{\sqrt{(1-r)^2 A^2 + H^2}},$$

we obtain

$$\psi_\xi = \psi_\eta = 0, \qquad \text{on side } \overline{QO}. \tag{12}$$

Equations (4),(5) and boundary conditions (7),(10)–(12) formulate a boundary value problem on the fundamental triangle.

3. NUMERICAL METHODS

The fundamental triangle POQ is covered by a uniform mesh with mesh size $h = 1/N$ in both ξ and η directions where N is a preassigned positive integer. In the following, we will denote the grid point by (i,j) (see Figure 2a), and in case of utilizing a 9-point stencil centered at (x,y), we denote points (x,y), $(x+h,y)$, $(x,y+h)$, $(x-h,y)$, $(x,y-h)$, $(x+h,y+h)$, $(x-h,y+h)$, $(x-h,y-h)$, $(x+h,y-h)$ by 0, 1, 2, 3, 4, 5, 6, 7, 8, respectively (see Figure 2b). As discussed in Section 1, the numerical schemes will be constructed in the computational region $\{(i,j) \mid 2 \leq j \leq N-1,\ 2 \leq i \leq N-j+1\}$, as illustrated in Figure 2a, where the interior points are marked by a circle and computational boundary points are marked by a solid disc.

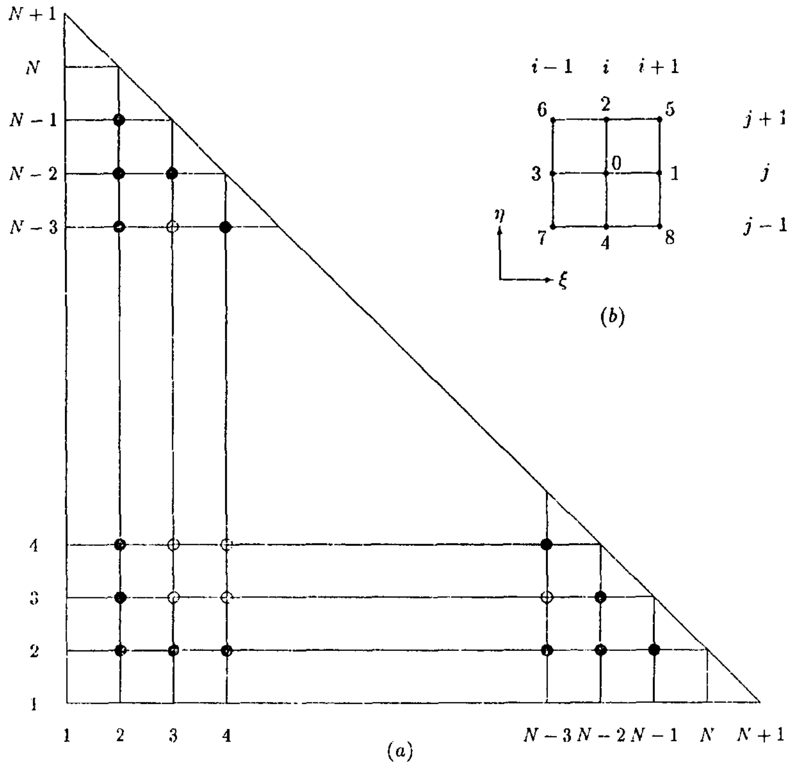

Figure 2. Grid network and 9-point stencil.

We shall derive the numerical schemes by second-order central difference formulas, namely in the 9-point stencil (see Figure 2b)

$$
\begin{aligned}
u_\xi &= \frac{(u_1 - u_3)}{2h} + O\left(h^2\right), & u_\eta &= \frac{(u_2 - u_4)}{2h} + O\left(h^2\right), \\
u_{\xi\xi} &= \frac{(u_1 + u_3 - 2u_0)}{h^2} + O\left(h^2\right), & u_{\eta\eta} &= \frac{(u_2 + u_4 - 2u_0)}{h^2} + O\left(h^2\right), \\
u_{\xi\eta} &= \frac{(u_5 - u_6 + u_7 - u_8)}{4h^2} + O\left(h^2\right). & &
\end{aligned}
\tag{13}
$$

Special care must be taken on the grid points nearest the hypotenuse of the fundamental triangle where point 5 is missing (outside the region of interest), so we need a difference formula for $u_{\xi\eta}$ in an 8-point stencil. The difference approximation in this kind of unsymmetric stencil has been documented in the literature; for example, see [9,10]. Let

$$
u_{\xi\eta} = \sum_{i=0}^{8} c_i u_i + O\left(h^2\right),
$$

and perform Taylor expansion at point 0 on each term in the summation up to $O(h^4)$. We then equate corresponding coefficients on two sides for all partial derivatives. This leads to a linear system of nine unknowns with nine equations. By choosing $c_5 = 0$, we obtain

$$c_0 = -\frac{1}{h^2}, \qquad c_1 = c_2 = c_3 = c_4 = \frac{1}{2h^2}, \qquad c_5 = c_6 = 0, \qquad c_7 = c_8 = -\frac{1}{2h^2},$$

which gives

$$u_{\xi\eta} = \frac{(u_1 + u_2 + u_3 + u_4 - 2u_0 - u_6 - u_8)}{2h^2} + O\left(h^2\right). \tag{14}$$

3.1. Finite Differences at Interior Grids

By using (13), numerical schemes for (4),(5) at interior points are straightforward:

$$\frac{C_1\left(\psi_1 + \psi_3 - 2\psi_0\right)}{h^2} + \frac{C_2\left(\psi_5 - \psi_6 + \psi_7 - \psi_8\right)}{4h^2} + \frac{C_3\left(\psi_2 + \psi_4 - 2\psi_0\right)}{h^2} = -r^2 H^2 \zeta_0, \tag{15}$$

$$\begin{aligned}\frac{C_1\left(\zeta_1 + \zeta_3 - 2\zeta_0\right)}{h^2} + \frac{C_2\left(\zeta_5 - \zeta_6 + \zeta_7 - \zeta_8\right)}{4h^2} + \frac{C_3\left(\zeta_2 + \zeta_4 - 2\zeta_0\right)}{4h^2}& \\ = \frac{rH\mathrm{R}}{A}\frac{\left((\zeta_1 - \zeta_3)(\psi_2 - \psi_4) - (\zeta_2 - \zeta_4)(\psi_1 - \psi_3)\right)}{4h^2}&,\end{aligned} \tag{16}$$

where

$$C_1 = 1 + \frac{H^2}{A^2}, \qquad C_2 = 2\left(r - 1 - \frac{H^2}{A^2}\right), \qquad C_3 = \left((r-1)^2 + \frac{H^2}{A^2}\right).$$

The exceptions are taking place on the interior points next to the computational boundary of the hypotenuse, i.e., points in the set $\{(i,j) \mid 3 \le j \le N-3,\ i = N-j\}$, where the values of ζ_5 are not available. In this case, we simply replace the C_2 term in (16) by using (14).

3.2. Numerical Boundary Conditions

We shall first specify stream function values on the computational boundaries as marked by solid discs in Figure 2a. Denote any point in the set $\{(i,j) \mid 3 \le j \le N-3,\ i = 2$ or $3 \le i \le N-3,\ j = 2\}$ and its adjacent points on physical boundary and in interior domain by II, I, and III, respectively. Using a Taylor expansion, we have

$$\psi_{\mathrm{II}} = \psi_{\mathrm{I}} + h\psi_{\mathrm{I}}' + \frac{h^2}{2}\psi_{\mathrm{I}}'' + O\left(h^3\right), \qquad \psi_{\mathrm{III}} = \psi_{\mathrm{I}} + 2h\psi_{\mathrm{I}}' + 2h^2 2\psi_{\mathrm{I}}'' + O\left(h^3\right).$$

By (7) and (11), $\psi_{\mathrm{I}} = \psi_{\mathrm{I}}' = 0$, we obtain

$$\psi_{\mathrm{II}} = \frac{1}{4}\psi_{\mathrm{III}} + O\left(h^3\right). \tag{17}$$

The rest of the boundary points (nearest to the moving side) will be linked with two adjacent points along the direction normal to the hypotenuse, one on physical boundary and another in interior. Let (x,y) be a point in the set $\{(i,j) \mid 3 \le j \le N-2,\ i + j = N+1\}$. By (7) and (10), we have

$$\psi\left(x + \frac{h}{2}, y + \frac{h}{2}\right) = 0, \qquad \psi_\xi\left(x + \frac{h}{2}, y + \frac{h}{2}\right) = \psi_\eta\left(x + \frac{h}{2}, y + \frac{h}{2}\right) = H.$$

Using Taylor expansion at $(x + h/2, y + h/2)$ gives

$$\psi(x,y) = 0 - \frac{h}{2}(H + H) + \frac{1}{2}\left(\frac{h}{2}\right)^2\left(\frac{\partial}{\partial\xi} + \frac{\partial}{\partial\eta}\right)^2\psi\left(x + \frac{h}{2}, y + \frac{h}{2}\right) + O\left(h^3\right),$$

$$\psi(x-h, y-h) = 0 - \frac{3h}{2}(H + H) + \frac{1}{2}\left(\frac{3h}{2}\right)^2\left(\frac{\partial}{\partial\xi} + \frac{\partial}{\partial\eta}\right)^2\psi\left(x + \frac{h}{2}, y + \frac{h}{2}\right) + O\left(h^3\right).$$

Eliminating h^2 terms yields

$$\psi_0 = \frac{1}{9}\psi_7 - \frac{2}{3}hH + O\left(h^3\right), \tag{18}$$

where we have again used the same notation as in Figure 2b. Obviously, (18) is directly applicable to the points in set $\{(i,j) \mid 3 \leq j \leq N-2,\ i+j = N+1\}$. For corner points $(2,2)$, $(2,N-2)$, $(2,N-1)$, $(N-1,2)$, and $(N-2,2)$, there are two ways to specify stream function value; i.e., the points can be linked to two different sides by the above techniques. We define stream function as the arithmetic average of the two specifications which can be regarded as a least-square fitting.

Specifying vorticity values on the computational boundary is relatively simple. For the points in set $\{(i,j) \mid 2 \leq i \leq N-2,\ j = 2 \text{ or } 3 \leq j \leq N-2,\ i = 2\}$, equation (15) is used to determine vorticity as each 9-point stencil is right within the physical domain. For points in set $\{(i,j) \mid 2 \leq j \leq N-1,\ i+j = N+1\}$ vorticity values are determined by (15) except that the approximation for $\psi_{\zeta\eta}$ in the C_2 term is replaced by (14).

3.3. Newton's Iteration Process

The finite difference discretization described in the previous sections will result in a system of nonlinear equations of $(N-1) \times (N-2)$ unknowns and same number of equations. A standard Newton's iteration process (see, e.g., [15]) is employed to solve the nonlinear system. The lexicographic ordering of the grid points is used so that the linearized Jacobian is a banded matrix which enables us to take advantage of the direct solvers for banded structure. It is also worth noting that the condition number of the Jacobian matrix depends on the formulation of the Navier-Stokes equations as well as the numerical schemes. An efficient Newton-like method for solving the square driven cavity using the fourth-order stream function Navier-Stokes equations is described by Schreiber and Keller [5]. It is found in [1,2] that a relatively straightforward generalization of the technique of Schreiber and Keller for the triangle problem resulted in linear systems which are so ill-conditioned that accurate numerical solutions are virtually impossible. In contrast, the present approach is shown to be very robust for a wide range of Reynolds numbers. Presumably this is due to the use of lower-order Navier-Stokes equations which makes the Jacobian matrix more well conditioned. In all our calculations, the Gaussian elimination process for linearized system runs smoothly and the quadratic convergence of Newton's iteration is well demonstrated, as only three to four Gaussian eliminations are required to reduce the r.m.s. error of the residuals to 10^{-5}.

4. NUMERICAL RESULTS

In this section, we present flow patterns and characteristic parameters for a triangular cavity with different shape and Reynolds numbers. The usual Reynolds-number-continuation is used to develop steady solutions for higher R, with the increment $\Delta\mathrm{R} = 50$ for $\mathrm{R} \leq 500$ and $\Delta\mathrm{R} = 100$ for $\mathrm{R} > 500$. At the very beginning ($\mathrm{R} = 1$), the initial values of stream function and vorticity are set to 0; afterwards for each iteration step, the initial guess is set to be the steady solution for the previous Reynolds number. Numerical tests for a variety of triangular geometries have been investigated, with R up to 1500 for equilateral cavity and 800 for scalene cavity, but for brevity, we shall only give here the detailed description for the equilateral cavity and one case of scalene cavity. It should be pointed out that the Reynolds number is based on $H/3$, which is consistent with the definition in [1,2] in the case of the equilateral cavity. In this case, if a side of the triangular cavity is used as the length scale, the actual R would be $2\sqrt{3}$ -fold, so $\mathrm{R} = 1500$ is equivalent to a conventional Reynolds number of 5196.

4.1. Equilateral Triangular Cavity

Consider the same geometry as in [1,2] with $A = \sqrt{3}$, $r = 2$, $H = 3$. This gives an equilateral cavity with length of each side $2\sqrt{3}$. Using mesh sizes $= 1/50$, $1/60$, $1/70$, and $1/80$, we obtain numerical results for a Reynolds number up to 1000. Detailed characteristic parameters are given in Tables 1 and 2. It can be seen from Table 1 that our results are in good agreement with those obtained by McQuain *et al.* [1]. Also the comparison between the coarse and fine mesh results show the reliability of using a coarse grid. Table 2 shows that as R is greater than 1000, the location of the center of the primary eddy seems to be independent of the Reynolds number. The streamlines and vorticity distributions for different Reynolds numbers are shown in Figures 3 and 4. It is observed that the interior of the primary eddy has almost constant vorticity for reasonably large R.

Table 1. Properties of the center of the primary eddy, located at (x_c, y_c) with stream function value ψ_c and vorticity ζ_c.

R	Source	ψ_c	ζ_c	x_c	y_c
	Present ($h = 1/50$)	0.235	1.368	1.767	2.460
1	Present ($h = 1/80$)	0.234	1.399	1.732	2.475
	McQuain *et al.* ($h = 1/200$)	0.233	1.363	1.749	2.460
	Present ($h = 1/50$)	0.240	1.527	2.113	2.460
50	Present ($h = 1/80$)	0.235	1.438	2.100	2.438
	McQuain *et al.* ($h = 1/200$)	0.237	1.464	2.078	2.445
	Present ($h = 1/50$)	0.253	1.349	2.044	2.340
100	Present ($h = 1/80$)	0.244	1.264	2.100	2.363
	McQuain *et al.* ($h = 1/200$)	0.247	1.373	2.061	2.355
	Present ($h = 1/50$)	0.269	1.212	1.940	2.280
200	Present ($h = 1/80$)	0.262	1.156	1.905	2.250
	McQuain *et al.* ($h = 1/200$)	0.260	1.272	1.940	2.280
	Present ($h = 1/50$)	0.277	1.124	1.905	2.220
350	Present ($h = 1/80$)	0.274	1.153	1.884	2.213
	McQuain *et al.* ($h = 1/200$)	0.268	1.232	1.905	2.265
	Present ($h = 1/50$)	0.279	1.066	1.871	2.160
500	Present ($h = 1/80$)	0.278	1.124	1.840	2.213
	McQuain *et al.* ($h = 1/200$)	0.269	1.250	1.905	2.265

Table 2. The feature of the vortex eddies in the equilateral triangular cavity at high Reynolds numbers. The results were obtained using $h = 1/80$.

	Primary vortex	Bottom vortex	Upper corner vortex
R	ψ, ζ, location	ψ, ζ, location	ψ, ζ, location
600	0.280, 1.110, (1.862, 2.175)	−0.0115, −0.5672, (1.559, 0.975)	−0.0002, −0.1451, (0.390, 2.475)
800	0.280, 1.077, (1.819, 2.175)	−0.0121, −0.5507, (1.581, 0.938)	−0.0013, −0.4403, (0.433, 2.550)
1000	0.279, 1.048, (1.840, 2.138)	−0.0125, −0.6779, (1.537, 0.938)	−0.0024, −0.5608, (0.455, 2.588)
1200	0.278, 1.024, (1.840, 2.138)	−0.0126, −0.6507, (1.559, 0.900)	−0.0033, −0.5081, (0.455, 2.588)
1400	0.277, 1.003, (1.840, 2.138)	−0.0125, −0.7209, (1.537, 0.863)	−0.0041, −0.6412, (0.433, 2.625)
1500	0.277, 0.998 (1.840, 2.138)	−0.0125, −0.7275 (1.537, 0.863)	−0.0045, −0.6393 (0.433, 2.625)

According to the mean square law, the theoretical value of vorticity at the primary vortex center is 1.054 for equilateral cavity with length of side $2\sqrt{3}$. This interior constant vorticity prediction is given by Batchelor [16]. Our numerical results suggest that the stream function value at the center of the primary eddy, ψ_c, converges to a constant, and its vorticity ζ_c is quite close to 1.054 as $R > 500$.

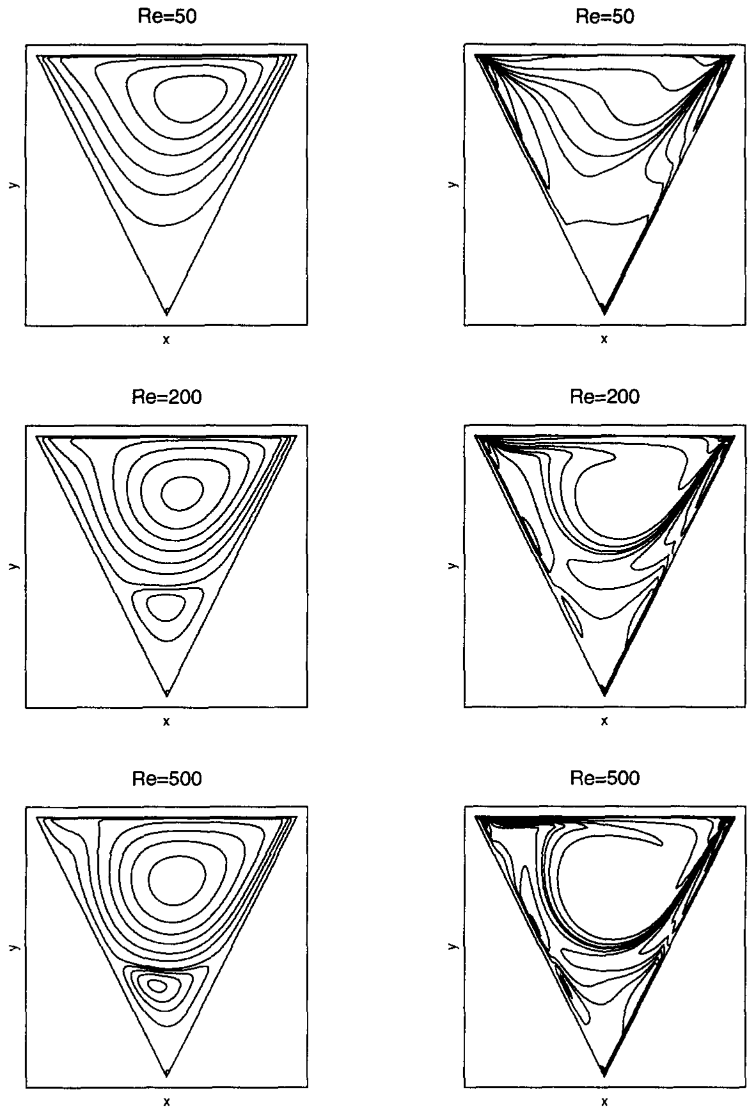

Figure 3. Streamlines and vorticity distributions for an equilateral triangular cavity at low-to-medium Reynolds numbers.

4.2. Scalene Triangular Cavity

Owing to the unsymmetric geometry, flow motion in scalene triangular cavity is very difficult to simulate. It was conjectured in [1,2] that it might be unavoidably ill conditioned. However, this type of motion may exist in practice despite being unstable. Its numerical investigation remains a challenge. In this section, we present a set of results for the so-called right-oriented triangular cavity by taking $A = 3\sqrt{3}/2$, $r = 4/3$, $H = 3$. By using mesh size $h = 1/50$, we could carry out the calculations for Reynolds numbers as high as 1000, but graphically only the results for $\mathrm{R} \leq 800$ are meaningful since oscillation appears in streamlines when R exceeds 800. Numerical results with finer meshes 1/70 and 1/80 are also obtained. It is found that the streamlines and vorticity contours with $h = 1/70$ are graphically indistinguishable from those obtained by using $h = 1/80$. In Figure 5, we plot the streamlines and vorticity contours for $\mathrm{R} = 100$, 500, 800 with a finer mesh $h = 1/80$. The feature of the vortex eddies are given in Table 3. Again it is seen that as R becomes large, the location of the center of the primary eddy and its stream function value seem to have converged.

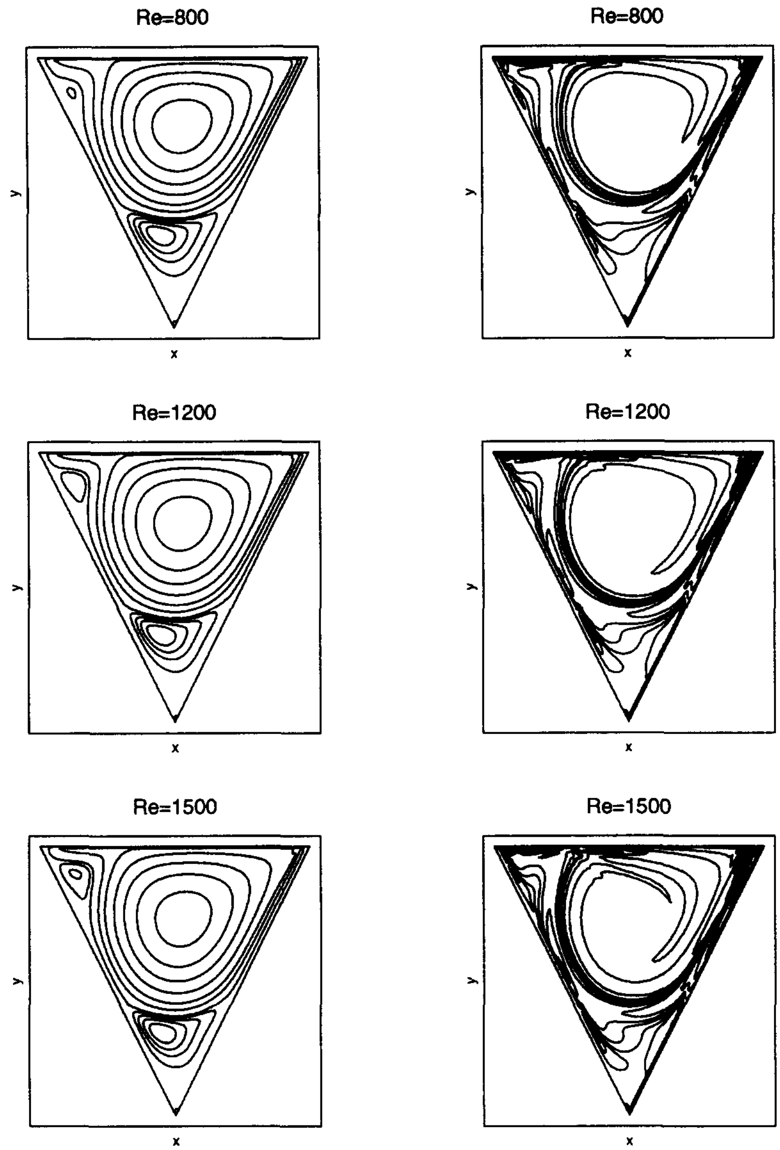

Figure 4. Streamlines and vorticity distributions for an equilateral triangular cavity at high Reynolds numbers.

Table 3. The feature of the vortex eddies in a right-oriented triangular cavity. The results were obtained using $h = 1/80$.

R	Primary vortex	Bottom vortex	Upper corner vortex
1	0.230, 1.400 (2.014, 2.475)		
50	0.243, 1.401 (2.338, 2.400)	−0.0002, −0.0215 (2.479, 0.638)	
100	0.256, 1.197 (2.306, 2.288)	−0.0015, −0.0880 (2.447, 0.825)	
200	0.270, 1.132 (2.200, 2.213)	−0.0053, −0.2521 (2.382, 0.900)	
350	0.279, 1.143 (2.187, 2.175)	−0.0086, −0.3852 (2.338, 0.900)	
500	0.277, 1.093 (2.187, 2.175)	−0.0102, −0.5158 (2.295, 0.900)	−0.0014, −0.3475 (0.736, 2.400)
600	0.273, 1.058 (2.187, 2.175)	−0.0108, −0.6384 (2.252, 0.900)	−0.0026, −0.4145 (0.750, 2.438)
700	0.272, 1.040 (2.176, 2.138)	−0.0111, −0.6377 (2.241, 0.863)	−0.0036, −0.4853 (0.758, 2.475)
800	0.270, 1.023 (2.176, 2.138)	−0.0114, −0.6914 (2.241, 0.863)	−0.0044, −0.4417 (0.758, 2.475)

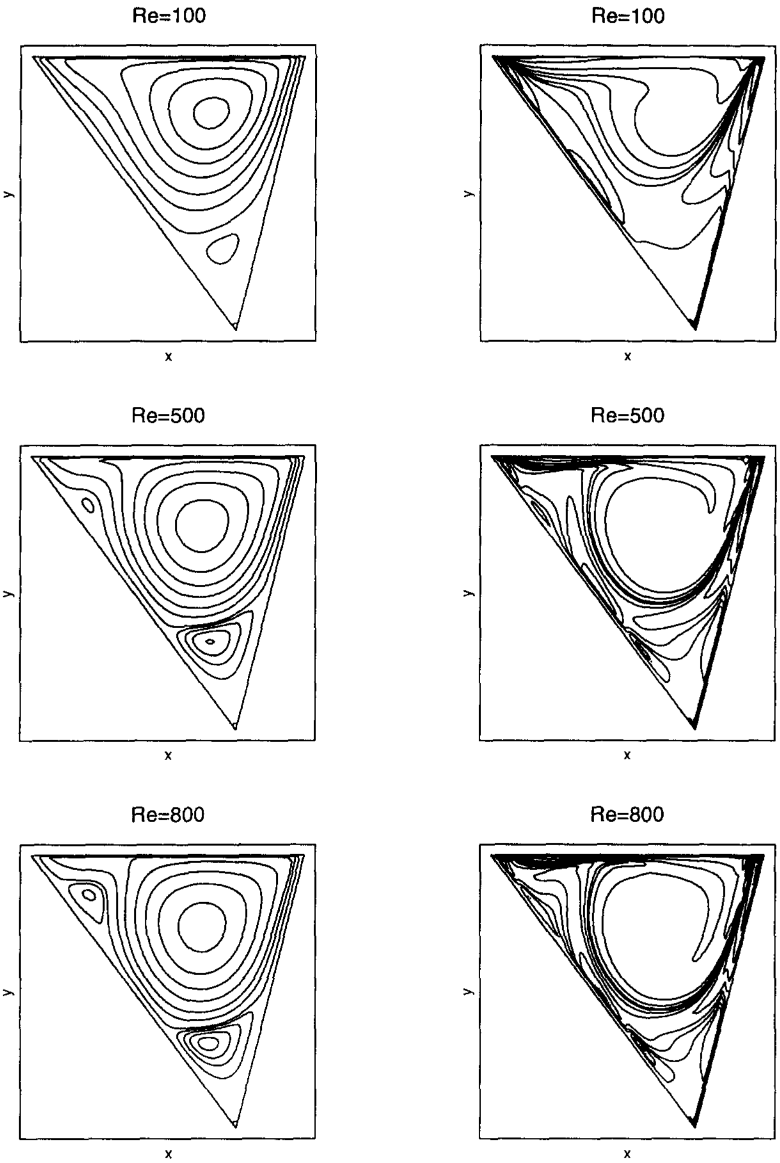

Figure 5. Streamlines and vorticity distributions for a right-oriented triangular cavity at different Reynolds numbers.

5. DISCUSSIONS AND CONCLUSIONS

We proposed a new approach to investigate the steady fluid flow in a triangular driven cavity. The advantage of our method is its improved efficiency due to the employment of the second-order Navier-Stokes equations. Our numerical scheme has been proved robust for a wide range of Reynolds numbers and applicable to triangular cavities with arbitrary shape. Reasonably accurate results can be obtained for Reynolds numbers up to 1000 by using only 50 mesh points in each direction. The coarse-mesh results compare reasonably well with the previous published results obtained by using 200×200 grids. It has been found that flow motion in an equilateral cavity is highly stable as in the case of a square cavity. Though our calculations stop at $R = 1500$, the solution procedure can be carried out for higher R without difficulty.

For time-independent Navier-Stokes equations, it has been found that Newton's iteration with a direct Jacobian matrix solver is very powerful for solving nonlinear systems resulting from the finite difference discretizations, especially when R is large. The use of Newton's process is advantageous over the usual SOR-like iterations in at least two aspects. It converges for a wide range of Reynolds numbers while SOR-like methods may often fail to converge at high R, and its quadratic convergence behavior prevents any possible temporal-type instabilities from developing in the artificial time of the SOR-like process for the steady problem [15]. The main disadvantage in using Newton's method is the high cost of CPU time and storage. However, this can be compensated by the fact that fairly nice results can be obtained by a relatively small number of grids, as demonstrated in this study.

Prior to the works of McQuain *et al.* and Ribbens *et al.*, it was believed that the condition number was not a serious problem in solving the linearized Jacobian system. In [1,2], it is found that a straightforward generalization of the technique of Schreiber and Keller [5] does not work for a triangular or a trapezoidal cavity problem. For moderate fine grids, the systems are numerically singular, with condition numbers in excess of 10^{13}. The ill-conditioning behavior is likely due to the use of the fourth-order Navier-Stokes equations. The present approach using a coupled system of two second-order equations proved quite successful and yielded accurate solutions for high Reynolds numbers. For most of our calculations, the systems are well conditioned with condition numbers in the order of 10^6. In all cases, at most four Newton iterations are required to reduce the r.m.s. error of the residuals to 10^{-5}.

REFERENCES

1. W.D. McQuain, C.J. Ribbens, C.-Y. Wang and L.T. Watson, Steady viscous flow in a trapezoidal cavity, *Comput. Fluids* **23**, 613 (1994).
2. C.J. Ribbens, L.T. Watson and C.-Y. Wang, Steady viscous flow in a triangular cavity, *J. Comput. Phys.* **112**, 173 (1994).
3. U. Ghia, K.N. Ghia and C.T. Shin, High-Re solutions for incompressible flow using the Navier-Stokes equations and a multi-grid method, *J. Comput. Phys.* **48**, 387 (1982).
4. H. Nishida and N. Satofuka, High-order solutions of square driven cavity flow using a variable-order multi-grid method, *Int. J. Numer. Methods Eng.* **34**, 637 (1992).
5. R. Schreiber and H.B. Keller, Driven cavity flows by efficient numerical techniques, *J. Comput. Phys.* **49**, 310 (1983).
6. M.S. Engelman, R.L. Sani and P.M. Gresho, The implementation of normal and/or tangential boundary conditions in finite element codes for incompressible fluid flow, *Int. J. Numer. Meth. Fluids* **2**, 255 (1982).
7. E.M. Sparrow and M. Charmchi, Heat transfer and fluid flow characteristics of spanwise periodic corrugated ducts, *Int. J. Heat Mass Transfer* **23**, 471 (1980).
8. C.N. Savvides and J.H. Gerrard, Numerical analysis of the flow through a corrugated tube with application to arterial prothesis, *J. Fluid Mech.* **138**, 129 (1984).
9. G. Birkhoff and R.E. Lynch, Some current questions on solving linear elliptic problems, *Numer. Math.* **57**, 527 (1990).
10. R.J. Leveque and Z. Li, The immersed interface method for elliptic equations with discontinuous coefficients and singular sources, *SIAM J. Numer. Anal.* **31**, 1019 (1994).
11. A. Mayo and A. Greenbaum, Fast parallel iterative solution of Poisson's and the biharmonic equations on irregular regions, *SIAM J. Sci. Statist. Comput.* **13**, 101 (1992).
12. H. Huang and H. Yang, The computational boundary method for solving the Navier-Stokes equations, Research report (unpublished), Institute of Applied Mathematics, University of British Columbia, Canada, (1990).
13. M. Li, T. Tang and B. Fornberg, A compact fourth order finite difference scheme for the steady incompressible Navier-Stokes equations, *Int. J. Numer. Methods Fluids* **20**, 1137 (1995).
14. P.M. Gresho, Incompressible fluid dynamics: Some fundamental formulation issues, *Annu. Rev. Fluid Mech.* **23**, 413 (1991).
15. B. Fornberg, Steady viscous flow past a circular cylinder up to Reynolds number 600, *J. Comput. Phys.* **61**, 297 (1985).
16. G.K. Batchelor, On steady laminar flow with closed streamlines at large Reynolds number, *J. Fluid Mech.* **1**, 177 (1956).